Hilbert-Glass Transition: New Universality of Temperature-Tuned Many-Body Dynamical Quantum Criticality

David Pekker,[1,2] Gil Refael,[1] Ehud Altman,[3,4] Eugene Demler,[5] and Vadim Oganesyan[6,7]

[1]*Institute of Quantum Information and Matter, Department of Physics, California Institute of Technology, Pasadena, California 91125, USA*

[2]*Department of Physics and Astronomy, University of Pittsburgh, Pittsburgh, Pensilvania 15260, USA*

[3]*Department of Condensed Matter Physics, Weizmann Institute of Science, Rehovot 76100, Israel*

[4]*Department of Physics, University of California, Berkeley, California 94720, USA*

[5]*Department of Physics, Harvard University, Cambridge, Massachusetts 02138, USA*

[6]*Department of Engineering Science and Physics, College of Staten Island, CUNY, Staten Island, New York 10314, USA*

[7]*The Graduate Center, CUNY, New York, New York 10016, USA*

(Received 20 September 2013; revised manuscript received 23 December 2013; published 31 March 2014)

We study a new class of unconventional critical phenomena that is characterized by singularities only in dynamical quantities and has no thermodynamic signatures. One example of such a transition is the recently proposed many-body localization-delocalization transition, in which transport coefficients vanish at a critical temperature with no singularities in thermodynamic observables. Describing this purely dynamical quantum criticality is technically challenging as understanding the finite-temperature dynamics necessarily requires averaging over a large number of matrix elements between many-body eigenstates. Here, we develop a real-space renormalization group method for excited states that allows us to overcome this challenge in a large class of models. We characterize a specific example: the 1 D disordered transverse-field Ising model with generic interactions. While thermodynamic phase transitions are generally forbidden in this model, using the real-space renormalization group method for excited states we find a finite-temperature dynamical transition between two localized phases. The transition is characterized by nonanalyticities in the low-frequency heat conductivity and in the long-time (dynamic) spin correlation function. The latter is a consequence of an up-down spin symmetry that results in the appearance of an Edwards-Anderson-like order parameter in one of the localized phases.

DOI: 10.1103/PhysRevX.4.011052

Subject Areas: Atomic and Molecular Physics, Condensed Matter Physics, Quantum Physics

I. INTRODUCTION

Our ability to describe emergent behavior in many-body systems relies, to a large extent, on the universality of critical phenomena associated with phase transitions and spontaneous symmetry breaking. Spontaneous symmetry breaking plays an important role even in disordered systems. For example, the spin-glass transition in classical magnets with random interactions follows this paradigm: as temperature drops, a specific frozen magnetization pattern that breaks an Ising symmetry emerges [1,2]. In one dimension, however, there are strong arguments, which forbid spontaneous symmetry breaking and, more generally, thermodynamic phase transitions from occurring at any nonvanishing temperature [3,4].

Do these arguments rule out the observation of critical phenomena in one-dimensional systems at nonvanishing temperature? A recent theoretical work, which generalizes the phenomenon of Anderson localization [5] to interacting many-body systems, suggests otherwise [6,7]. Its intriguing prediction is that an isolated many-body system subject to strong disorder can undergo a phase transition, from a state with strictly zero (thermal) conductivity at low temperature to a metallic phase above a critical temperature. This transition has only dynamical manifestations and no thermodynamic ones, and is, in this sense, a many-body extension of the mobility edge [8] in the Anderson localization transition in 3 D. A similar many-body transition was also suggested to exist in the 1 D bosonic case [9], at infinite temperatures as a function of disorder strength [10–12], and in quasiperiodic systems without disorder [13]. Very little, however, is known about the universality of such transitions.

In this paper, we uncover a wider class of unconventional critical phenomena, whose existence was hinted by the many-body localization transition example. By

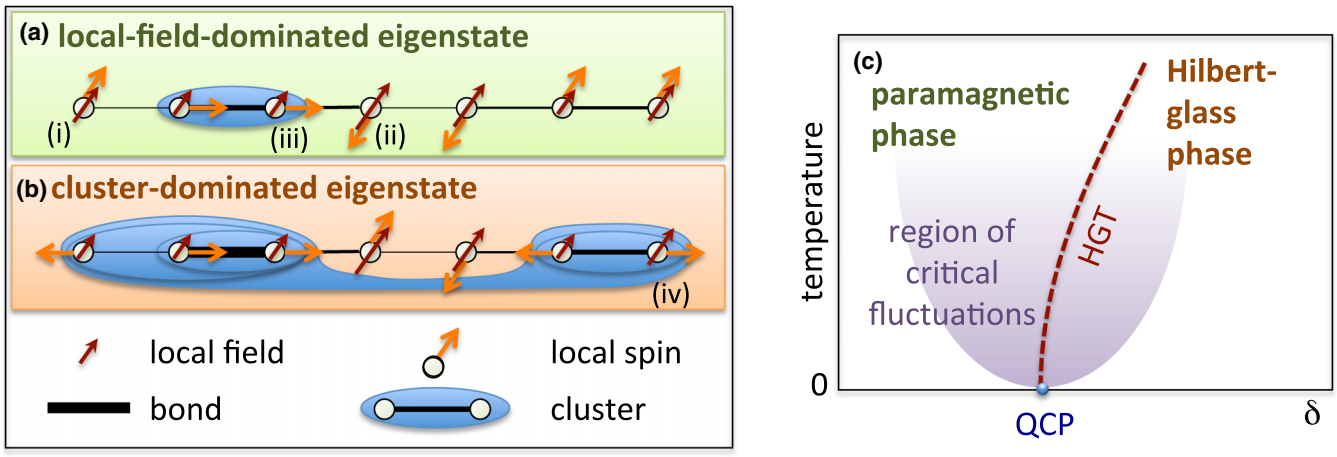

FIG. 1. (a) Schematic representation of a typical eigenstate in the paramagnetic (local-field-dominated) phase: the local spins are largely aligned (i) or antialigned (ii) with the local fields; rare clusters can still be present (iii). (b) Hilbert-glass (cluster-dominated) eigenstate: local spins form magnetic clusters that often contain domain walls; rare isolated spins can still be present. (c) Schematic phase diagram of the Hilbert-glass transition (HGT) in the tuning parameter–temperature plane. The diagram shows the HGT line separating the paramagnetic (local-field-dominated) and the Hilbert-glass (cluster-dominated) phases terminating in a zero-temperature quantum critical point (QCP). The behavior of equilibrium thermodynamic observables at finite temperatures is governed by the QCP in the region of critical fluctuations [15]. While equilibrium thermodynamic observables have no singularities in the phase diagram, with the exception of the zero-temperature QCP, dynamical observables show singular behavior along the HGT line.

investigating a random spin chain with generic interactions, we find and characterize another instance of this new class of transitions that exhibit nonanalytic dynamical behavior as a function of temperature but lack any strictly thermodynamic signatures. The transition stems from the structure of the many-body eigenstates, which decidedly changes as we tune the extensive many-body energy [14]. On one side of the transition (the paramagnetic side) the eigenstates consist of most spins aligned or antialigned with the random local field, while on the other side (the glass side) spins show a pattern of frozen magnetization that breaks a $\mathbb{Z}_2$ symmetry [see Figs. 1(a) and 1(b)]. The magnetization pattern is random, however, and varies from eigenstate to eigenstate as if each is a classical spin-glass ground state of a different disorder realization. The signatures of the phases and phase transition appear not in a single state, but rather in a large portion of the many-body Hilbert space. Therefore, we coin the term Hilbert-glass transition (HGT) to describe this type of dynamical quantum criticality. The properties of the HGT are summarized in the generic phase diagram, Fig. 1(c).

The challenges for analyzing the HGT are clear: a complete knowledge of the properties of an entire excitation spectrum—wave functions and energies alike—is necessary. Previous efforts to characterize quantum dynamical transitions, such as the many-body localization transition, relied on exact diagonalization (ED) of small systems [10,12,16–22]. Here, we pursue an alternative approach based on the strong disorder real-space renormalization group (RSRG) method [23–28] and its extensions to unitary time evolution [29]. We generalize the method to deal with arbitrary-energy excitations, hence, the acronym RSRG-X. The RSRG-X allows us to investigate the dynamics of an arbitrary-temperature thermal state of strongly disordered systems containing thousands of sites, i.e., accessing systems 2 orders of magnitude larger than what exact diagonalization can access.

Unlike the many-body localization transition, the transition we describe occurs between two localized phases, which, therefore, cannot thermalize on their own [30–32]. Nonetheless, there are physical settings in which it is meaningful to discuss thermal response functions and temperature-tuned transitions in these systems. First, one can imagine preparing the system in equilibrium by connecting it to an external bath, which is adiabatically disconnected before the start of the response measurement. Alternatively, the system could be weakly coupled to a thermal bath at all times. In the second case there is a time scale, set by the bath coupling strength, beyond which the bath dominates the dynamics. The strong-disorder fixed point that we describe would provide a faithful description of the dynamical behavior on shorter time scales.

The model we investigate with the RSRG-X is the generalized quantum Ising model

$$\mathcal{H}_{\mathrm{hJJ'}} = -\sum_i (J_i \sigma_i^x \sigma_{i+1}^x + h_i \sigma_i^z + J_i' \sigma_i^z \sigma_{i+1}^z). \qquad (1)$$

Without the last J' term, Eq. (1) represents the usual transverse-field Ising model (TFIM), which was the first arena in which real-space renormalization group was used to elucidate the novel universal properties of phase transition dominated by strong disorder [25,27]. In particular, the RSRG analysis yields the infinite randomness energy-length scaling $\log(1/E) \sim \ell^{1/2}$, in contrast to the $E \sim \ell^{-z}$ scaling in conventional critical systems.

The TFIM makes a natural starting point for investigating dynamical critical points in strongly disordered systems. The TFIM, Eq. (1), however, can be mapped to a free fermion theory, making its dynamics fundamentally equivalent to that of a certain class of single-particle Anderson localization (with particle-hole symmetry). We avoid this problem by adding the J' interaction term, which preserves the $\mathbb{Z}_2$ symmetry, while making the model intrinsically interacting. It has been shown that the dynamics in the many-body localized phase, i.e., in the presence of interactions, can be different than in the noninteracting case [20–22,29,33].

The paper is organized as follows. In Sec. II, we develop the RSRG-X procedure and consider the flows it produces. The flows reveal the evolution of the many-body eigenstate structure as temperature is varied, which allows us to identify the dynamical phase transition and construct the phase diagram. We find that the temperature-tuned transition is controlled by an infinite-randomness critical point, with the same scaling properties as the zero-temperature quantum phase transition [25]. In Secs. III and IV, we examine two dynamical observables: the low-frequency spin autocorrelation function (and an associated Edwards-Anderson-type order parameter) and the frequency-dependent thermal conductivity. Using the RSRG-X, we find that in the vicinity of the critical temperature, both observables show scaling behavior consistent with the infinite-randomness critical point. The scaling behavior becomes nonanalytic in the infinite system-size limit. Finally, we discuss the implications of our results in Sec. V.

II. DYNAMICAL PHASE DIAGRAM OF THE hJJ′ MODEL

Our task is to develop a renormalization group procedure suited for describing the excited states of the weakly interacting hJJ′ model. Our approach is based on the core ideas of the RSRG methods developed for the ground state behavior of random magnets [23–26,28], and for the TFIM, in particular [27]. In the ground state methods, at each RSRG step we diagonalize the strongest local term of the Hamiltonian [Eq. (1)] and fix the corresponding subsystem in the ground eigenstate of that term. We generate effective couplings between the subsystem and its neighboring spins through second-order perturbation theory, allowing only virtual departures from the chosen ground state of the strong term. In the TFIM, when the nearest-neighbor x-x interaction is dominant, the RSRG steps lead to the formation of a macroscopic ferromagnetic cluster that breaks the Ising symmetry. On the other hand, when the transverse field is dominant, it pins most local spins to the $+z$ direction. The addition of weak interactions, $J_i' \ll J_i$, h_i, results in a shift of the critical point but cannot affect the universal zero temperature properties of the TFIM.

A. RSRG-X

The crucial difference between our RSRG-X method and the ground state RSRG methods has to do with the choice of the local eigenstates at each RG step. Instead of retaining only the lowest energy states at each RG step, we can choose either the low-energy or the high-energy manifold of the local term. The two manifolds are separated by a large gap, which controls the perturbation theory with which we generate the effective couplings. Thus, each RSRG-X step corresponds to a binary branching of a tree, as illustrated in Fig. 2(a), where the leaves of the tree correspond to the actual many-body spectrum, Fig. 2(b).

Implementing the RSRG-X on the hJJ′ model requires two types of RG decimation steps: site and bond decimations. Consider the nth RSRG-X step. If the largest gap in the system is due to a field h_2 [see Fig. 2(c)], the site could

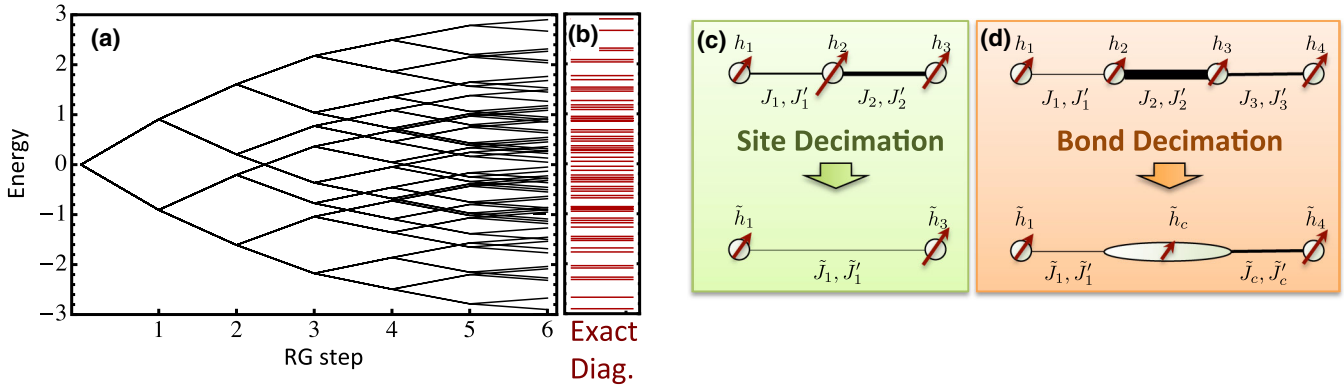

FIG. 2. (a) The RSRG-X tree for a six-site Ising chain. The leaves of the tree correspond to the many-body eigenstates of the spin chain. (b) The corresponding eigenspectrum found by exact diagonalization. (c),(d) RSRG-X rules for site (c) and bond (d) decimation in the hJJ′ model. In the site decimation rule, a local magnetic field (h_2) is the dominant coupling; thus, the corresponding local spin is either aligned (ground state) or antialigned (excited state) with it. Eliminating h_2, we obtain a new set of couplings $\tilde{h}_1$, $\tilde{J}_1$, $\tilde{J}_1'$, and $\tilde{h}_3$ to second order (see Appendix B for details). In the bond decimation rule, J_2 is the dominant coupling, corresponding to the neighboring spins being either aligned (ground state) or antialigned (excited state, i.e., a domain wall) along the x axis.

be eliminated by letting spin 2 be either mostly aligned ($c_n = +1$) or mostly antialigned ($c_n = -1$) with the local field. Second-order perturbation theory induces an effective Ising coupling between sites 1 and 3: $\tilde{J} \to c_n J_1 J_2 / h_2$. Additionally, J' couplings shift the local fields $\tilde{h}_{1(3)} \to h_{1(3)} + c_n J'_{1(2)}$. The significance of these shifts is that subsequent RSRG-X steps depend on the history of branching c_n's at all higher energy scales. The history dependence is a feature of the interacting model and would not arise in the case $J'_i = 0$. If the largest gap is due to a bond J_2 [see Fig. 2(d)], the two sites 2 and 3 form a cluster that is either ferromagnetic ($c_n = +1$) or antiferromagnetic ($c_n = -1$). The rules for cluster formation also follow from second-order perturbation theory. See Appendix A for a detailed derivation of the RSRG-X framework using Schrieffer-Wolff transformations and Appendix B for the application of the framework to the hJJ′ model. Because of our choice of the initial distributions, throughout the RSRG-X flow all J' values are small compared to the nearby J and h values, and, therefore, we do not implement a J' elimination step. Once we have eliminated the largest term in the Hamiltonian, we reduce the scale of the largest gap, and then seek the next largest gap, until all degrees of freedom in the chain are eliminated.

Obtaining the entire many-body spectrum requires the construction of all branches of the tree, which is an exponentially hard task. We, therefore, perform thermal sampling of typical eigenstates using the Monte Carlo method. In our procedure, Monte Carlo states correspond to the many-body eigenstates, which we describe via a sequence of branching choices $b = \{c_1, c_2, \ldots, c_L\}$ going from the root to a leaf of the tree, where L is the number of sites in the chain. To obtain a new Monte Carlo state b', we start at the leaf of the tree, go up the tree a random number of nodes, e.g., m, and flip $c_{L-m} \to -c_{L-m}$. Next, we calculate the energy change of the many-body state due to the flip of c_m, by performing the RSRG-X steps from m to L, and accept or reject the new state b' according to METROPOLIS [34] (see Appendix C for details of our implementation of the numerics).

A possible concern regarding the RSRG-X method is that it fails to correctly account for resonant coupling between nearly degenerate but distinct branches, which could result in delocalization. Reference [29] has argued that, in the presence of strong disorder, these resonances are not strong enough to lift the near degeneracy of the eigenstates; hence, our system always remains localized.

B. RSRG-X flows

The dynamical phase diagram of the hJJ′ model derives from the flow of the full distributions of coupling constants h, J, and J'. We can, however, characterize the flow by tracking just two parameters: $\mathcal{C} = [\![\langle \mathrm{avg}[\ln|h|] - \mathrm{avg}[\ln|J|]\rangle_{\mathrm{Th}}]\!]$ and $\mathcal{D} = [\![\langle \mathrm{var}[\log|h|] + \mathrm{var}[\log|J|]\rangle_{\mathrm{Th}}]\!]$, where $\langle\cdots\rangle_{\mathrm{Th}}$ and $[\![\cdots]\!]$ represent thermal and disorder averaging. Because J' is irrelevant in the RG sense, we do not explicitly characterize the flow of the J' distribution. $\mathcal{C}$ measures the relative strength of h and J distributions: $\mathcal{C} > 0$ indicates that h's are dominant and the flow is towards the paramagnetic phase while $\mathcal{C} < 0$ indicates that J's are dominant and the flow is towards the Hilbert glass. $\mathcal{D}$ measures the disorder strength, which always grows upon coarse graining. In the $J' = 0$ case, the ratio $\delta = \mathcal{C}/\mathcal{D}$ remains almost constant throughout the RG flow [27], and, hence, we use the initial value of δ_I as a tuning parameter.

A peculiar property of the interaction-free TFIM (i.e., $J'_i = 0$) is that the absolute values of the effective couplings following any decimation are insensitive to the choice of final state (i.e., independent of c_n's). Therefore, the fate of the RSRG-X flow is solely determined by δ_I. Hence, the model experiences a dynamical transition at a fixed critical value of δ_I independent of temperature: $\delta_I > 0$ results in h-dominated flows towards the paramagnet while $\delta_I < 0$ results in J-dominated flows towards the Hilbert glass.

When interactions are added, temperature starts playing an important role because gaps produced by decimation steps are no longer independent of the choice of eigenstate. Thermal averaging biases decimation steps towards low or high energies, when $\beta = 1/T$ is positive or negative, respectively. This leads to a temperature-driven dynamical transition, which is the focus of this work. The transition is encoded in the flows shown in Fig. 3(a): fixing δ_I, we observe that the inverse temperature β tunes whether the flow is towards the Hilbert glass or the paramagnet.

C. Dynamical phase diagram

The flows obtained from the RSRG-X method reveal a dynamical phase diagram of the hJJ′ model. In Fig. 3(b) we display several cross sections of the phase diagram in the space of detuning versus inverse temperature for various values of the interaction strength. We describe the strength of the interactions by the parameter $\Delta_{J'}$, which measures the width of the J'_i distribution; $\Delta_{J'} > 0$ ($\Delta_{J'} < 0$) corresponds to the initial distribution with all $J'_i > 0$ ($J'_i < 0$). As $\Delta_{J'}$ (and, hence, typical J') decreases, the sigmoid phase transition curve narrows, becoming vertical at the noninteracting point $J' = 0$ and finally mirroring itself for negative values of $\Delta_{J'}$.

The shape of the phase diagram can be understood by noting the effect of the site decimation RG rule on the initial distributions (we always use $J_i > 0$, $h_i > 0$). When $\Delta_{J'} > 0$, J' increases h on neighboring sites in the excited state branches and reduces it in the low-energy branches. Tuning the temperature changes the branching ratios, which effectively alters the tuning parameter δ_I. Hence, we expect the shape of the transition line to be $\delta_I \approx C_0 \Delta_{J'} \tanh(E_{\mathrm{char}}/T_c)$, where T_c is the critical temperature, E_{char} is the characteristic energy scale describing

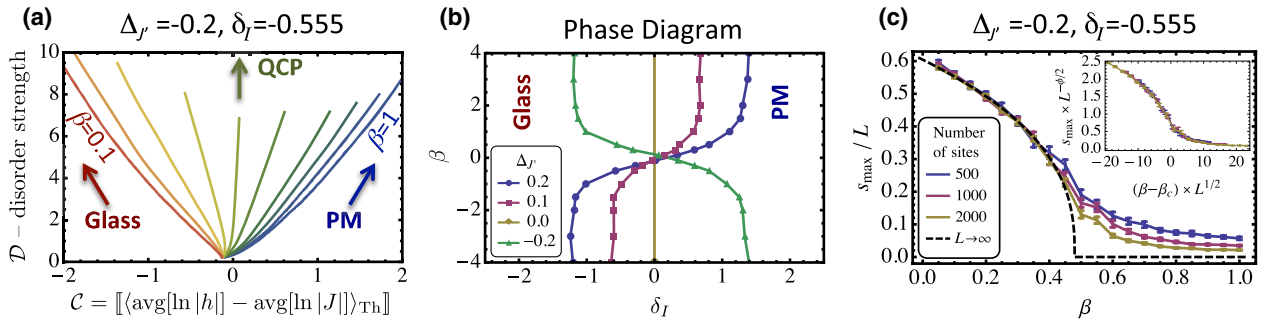

FIG. 3. (a) Renormalization group flows in the $\mathcal{C}$-$\mathcal{D}$ plane, where $\mathcal{C}$ measures whether local fields or bonds are stronger while $\mathcal{D}$ measures the strength of disorder. Tuning β results in RSRG-X flows towards the Hilbert-glass phase, the quantum critical point, and the paramagnetic phase (PM), as indicated by arrows. (The initial value of the tuning parameter δ and the width of the initial J' distribution $\Delta_{J'}$ is held fixed; see text.) (b) Phase diagram of the hJJ′ model in the δ-β plane for several values of $\Delta_{J'}$. (c) Size of the largest cluster $s_{\max}$ as a function of β for several values of the system size L. The transition becomes sharper and sharper as L increases. The inset shows a finite-size scaling collapse of the same data. (Error bars indicate uncertainty due to disorder averaging; uncertainty due to Monte Carlo sampling is always smaller.)

the initial J and h distributions, and C_0 is a constant related to the shape of the initial J' distribution. With the exception of a small offset, this shape is indeed observed in Fig. 3(b).

The offset can be understood from the infinite temperature limit: $\beta \to 0$ brings about an equal superposition of all branches, which washes away any J' effects. The remaining J'^2 effects, associated with the flow of $\langle \log h \rangle$, displace the transition line from the origin:

$$\delta_{I,c}(\beta \to 0) = C_0 E_{\mathrm{char}} \beta_c \Delta_{J'} + C_2 \Delta_{J'}^2, \tag{2}$$

where C_2 is also constant.

III. DYNAMICAL SPIN CORRELATIONS AND THE ORDER PARAMETER

Armed with the RSRG-X method, we now characterize the two dynamical phases and the phase transition between them. In the Hilbert-glass phase, the many-body eigenstates tend to contain an infinite cluster that is produced by bond decimations. We can crudely think of these eigenstates as having a random sequence of fixed values of σ^x on the different sites belonging to the infinite cluster. Thus, each eigenstate breaks the $\mathbb{Z}_2$ symmetry of the Ising model. Of course, different eigenstates, even very close in energy, typically have completely different spin configurations.

A natural signature of the cluster phase is the dynamic spin autocorrelation function

$$[\![\gamma(t)]\!] \equiv [\![\sum_n \frac{e^{-E_n/T}}{Z} \langle \psi_n \sigma_i^x(t) \sigma_i^x(0) \rangle \psi_n]\!]. \tag{3}$$

For an infinite system, in the cluster phase we expect this correlator to saturate: $\lim_{t\to\infty} [\![\gamma(t)]\!] \to f$, where $f = s_{\max}/L$ is the ratio of the number of sites participating in the largest cluster over the bare size of the chain [35]. Alternatively, the glass order parameter introduced by Edwards and Anderson (EA) can capture this kind of static eigenstate order and, moreover, survive thermal averaging

$$m_{\mathrm{EA}} \equiv [\![\sum_n \frac{e^{-E_n/T}}{Z} |\langle \psi_n \sigma_i^x \rangle \psi_n|^2]\!]. \tag{4}$$

It is important to note that, although the EA order parameter offers a static signature of the phase, it is not a thermodynamic observable [36] and, hence, does not entail a thermodynamic singularity.

To quantify the transition, we use RSRG-X to directly measure the fraction of the system occupied by the largest cluster $s_{\max}/L$. Figure 3(c) shows the evolution of the largest cluster fraction across the phase transition, as we tune the temperature. As the system size increases, the transition becomes sharper, approaching the $L \to \infty$ asymptote indicated by the dashed line. Indeed, this notion can be made concrete using a finite-size scaling hypothesis,

$$s_{\max} = L^{\phi/2} f[(\beta - \beta_c)^{1/\nu} L], \tag{5}$$

to successfully collapse the $s_{\max}$ data [see inset of Fig. 3(c)]. To obtain this hypothesis, we use the intuition that temperature (β) tuning is equivalent to δ_I tuning combined with two zero-temperature results: (1) correlation length critical exponent $\nu = 2$ and (2) at criticality $s_{\max} \sim L^{\phi/2}$ (where ϕ is the golden ratio) [26].

IV. LOCALIZATION AND HEAT CONDUCTIVITY

Transport measurements are an important experimental tool that could be used for the detection of dynamical phase transitions. Here, we present the first calculation of heat

transport using RSRG methods. We focus on the heat transport since the energy current is the only locally conserved current in the hJJ′ model. It is important to note that both the Hilbert glass and the paramagnetic phases are many-body localized. They do not thermalize by themselves and feature strictly vanishing dc heat conductivity. Nevertheless, it is interesting to characterize these phases by their ac transport in the low-frequency limit.

The calculation of the heat conductivity for the hJJ′ chain is a potent demonstration of the RSRG-X's strength. Using detailed knowledge of the local decimation steps leading to each branch in the many-body state tree, we can construct the Kubo integral (see Appendix D), which yields the real part of the conductivity:

$$\kappa(\omega) = \frac{1}{i\omega L}\sum_{i,j}\int_{-\infty}^{0} dt e^{-i\omega t}\langle[j_i(t), j_j(0)]\rangle_{\mathrm{Th}}. \qquad (6)$$

Here, $j_i(t) = [\sum_{k=1}^{i-1}\mathcal{H}_i, \mathcal{H}]$ is the energy current operator and $\mathcal{H}_k$ the Hamiltonian pertaining to site k and the bond k, $k+1$. Plotting the low-frequency heat conductivity as a function of β [see Fig. 4(a)], we observe a cusplike feature signaling the onset of the Hilbert-glass transition.

To understand the origin of this feature, and how it becomes sharper as $\omega \to 0$, we consider the scaling of $\kappa(\omega)$. In the noninteracting case, subsequent RSRG-X steps are independent of the preceding steps, and, hence, we can obtain (see Appendix D)

$$\kappa(\omega) \sim \omega^{\alpha}. \qquad (7)$$

At criticality, $\alpha = 3$, which is the engineering dimension of $\kappa(\omega)$. As we tune away from criticality, we observe the appearance of an anomalous dimension $\alpha \sim 3 + \mathrm{const}|\delta_I|$ (up to logarithmic corrections; see Appendix D). As J' is an irrelevant operator, we expect this scaling to persist in the presence of J'. Furthermore, using the equivalence of β and δ_I tuning, we hypothesize that $\alpha \sim 3 + \mathrm{const}|\beta - \beta_c|$ when we tune across the transition using temperature.

We test our scaling hypothesis in two ways. First, we plot κ for a small fixed ω as a function of β on semilog axes [see inset of Fig. 4(a)]. We observe essentially linear behavior away from the transition that is consistent with the hypothesis. Second, in Fig. 4(b), we plot $\kappa[\omega]$ as a function of ω for several values of temperature. $\kappa[\omega]$ displays nonuniversal behavior at high frequencies, which becomes a power law at low frequencies, and is cut off by the system size at very low frequencies. As we tune β towards the transition from either side, we observe that the power-law exponent α decreases, reaching its lowest value of 3.3 at the critical point [see inset of Fig. 4(b)]. Thus, up to logarithmic corrections that likely account for the deviation away from the engineering value $\alpha = 3$ in our 2000 site spin chain, we find that our numerical results are consistent with the expected critical scaling at the transition.

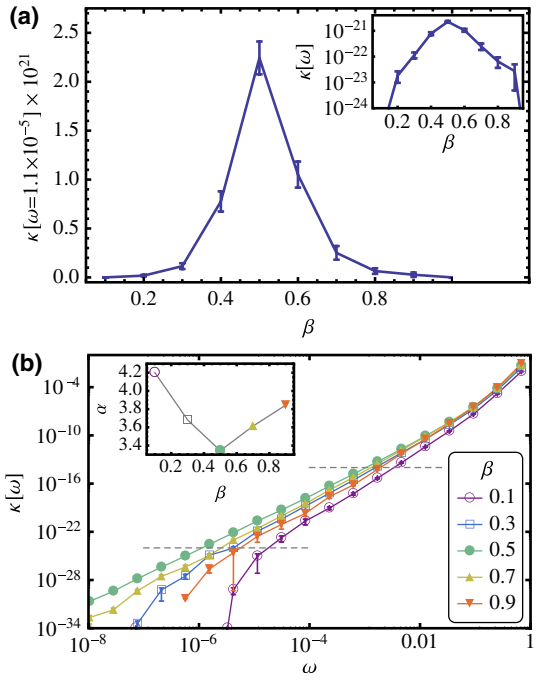

FIG. 4. (a) Low-frequency heat conductivity plotted as a function of temperature. At the phase transition, the system becomes least localized, which is associated with a cusp in the heat conductivity. Inset: Same data plotted on a log-linear scale supporting the form $\kappa \sim e^{-\mathrm{const}|\beta-\beta_c|}$. (b) Heat conductivity plotted as a function of frequency for five different temperatures. The low-frequency heat conductivity displays power-law scaling with frequency $\kappa(\omega) \sim \omega^{\alpha}$. Inset: α as a function of β (see text). [In all cases, $\delta_I = -0.555$ and $\Delta_{J'} = -0.2$. Error bars indicate uncertainty due to disorder averaging; uncertainty due to Monte Carlo sampling is always smaller. Dashed lines in (b) indicate the region being fitted for the inset.]

V. CONCLUSIONS

We have explored the notion of a dynamical finite-temperature transition by investigating a concrete model: the hJJ′ model. This investigation is made possible by the development of the RSRG-X, which we also describe in this paper. Although notions of a dynamical finite-temperature phase transition have appeared in the literature before, we offer a detailed description of a specific example of this type of transition.

Specifically, in the thermodynamic sense, the hJJ′ model has a 0^+ and a 0^- temperature quantum phase transition. Away from these two zero-temperature phase transitions, the model displays no singularities in any of its thermodynamic observables. However, connecting this pair of quantum critical points, we find the HGT line, associated with singular behavior in dynamical observables including dynamical spin autocorrelations and heat conductivity.

We, therefore, add a new type of universality to the lore of critical phenomena.

Finally, we note that the RSRG-X method could find applications in describing many-body eigenstates, especially localized eigenstates, in other models both in 1 D and in higher dimensions.

ACKNOWLEDGMENTS

It is our pleasure to thank Kedar Damle, Olexei Motrunich, David Huse, and Stefan Kehrein for useful conversations. The authors thank the KITP and the National Science Foundation under Grant No. NSF PHY11-25915 for hospitality during the conception of the paper and the Aspen Center for Physics and the NSF Grant No. 1066293 for hospitality during the writing of this paper. The computations in this paper were run on the Odyssey cluster supported by the FAS Science Division Research Computing Group at Harvard University. The authors acknowledge support from the Lee A. DuBridge prize postdoctoral fellowship (D. P.), the IQIM, an NSF center supported in part by the Moore Foundation (D. P., G. R.), DMR-0955714 (V. O.), the Packard Foundation (G. R.), BSF (E. A., E. D.), ISF and the Miller Institute for Basic Science (E. A.), Harvard-MIT CUA, the DARPA OLE program, AFOSR MURI on Ultracold Molecules, and ARO-MURI on Atomtronics (E. D.).

Note added.—Recently, a paper describing a method that has some similarities to our RSRG-X appeared [37]. Another paper posted in parallel to this one explores the HGT from the complementary viewpoint of the time evolution following a quench [38].

APPENDIX A: RSRG-X GENERAL FRAMEWORK

Our results rely on the extension of the real-space renormalization group to obtain and sample the excited spectrum of a 1 D problem. The method, which we refer to as RSRG-X, follows closely the ground-state-relevant constructions in Refs. [23–27]. In both cases, we iteratively eliminate the strongest local pieces of the Hamiltonian and construct the many-body state as an approximate tensor product of eigenstates of the strong terms. New low-energy terms arise during the elimination process, and they are calculated within second-order perturbation theory via a Schrieffer-Wolff transformation. The method concludes when all degrees of freedom are eliminated, or when the Hamiltonian consists only of mutually commuting terms.

We describe a single iteration step of the RSRG-X method. Our analysis assumes local Hamiltonians of the following form:

$$\mathcal{H} = \sum_i \mathcal{H}_{i/2}, \tag{A1}$$

where the terms with an integer index pertain to a site, and the terms with a half-integer index pertain to bonds, and have a nontrivial effect on the tensor product of the two Hilbert spaces of the appropriate two neighboring sites. The first task in the RSRG-X elimination step is to separately solve the local Hamiltonians $\mathcal{H}_{i/2}$ and find the term $\mathcal{H}_{m/2}$ with the largest energy gap in its spectrum.

Next, we concentrate on the three pieces $\mathcal{H}_{m/2,(m\pm1)/2} = \mathcal{H}_{(m-1)/2} + \mathcal{H}_{m/2} + \mathcal{H}_{(m+1)/2}$ and partially solve for the many-body ground state using a Schrieffer-Wolff transformation. We assume that the largest gap separates the energies of two subspaces of the domain of $\mathcal{H}_m$; we denote them with the letters a and b, and also define P_a and P_b as projections onto them. For convenience, we rewrite the three-term Hamiltonian in the following way:

$$\mathcal{H}_{m/2,(m\pm1)/2} = H_0 + V. \tag{A2}$$

$\mathcal{H}_0$ encodes the largest gap we identified and ignores all the degeneracy-breaking effects within the high- and low-energy subspaces. Without loss of generality, we write H_0 as

$$H_0 = \frac{\lambda}{2}\begin{pmatrix} I_a & 0 \\ 0 & -I_b \end{pmatrix}, \tag{A3}$$

where λ is the size of the largest local gap, and I_a and I_b are two identity matrices with dimensions corresponding to the dimension of the subspaces a and b. Our goal is to find a unitary transformation e^{iS}, such that

$$[e^{iS}(H_0 + V)e^{-iS}, H_0] = 0, \tag{A4}$$

i.e., that eliminates the pieces in V that mix the subspaces a and b. We perform this task perturbatively, expanding $S = S^{(0)} + S^{(1)} + S^{(2)} + \cdots$ in powers of V.

To facilitate the task, we introduce the notation that P_α is a projection onto subspace $\alpha \in \{a, b\}$, $P_{\bar{\alpha}}$ is the projection onto the complementary subspace, $(-1)^a = 1$, and $(-1)^b = -1$. $S^{(0)} = 0$ since H_0 does not connect the two subspaces. $S^{(1)}$ is found by solving $P_\alpha([iS^{(1)}, H_0] + V)P_{\bar{\alpha}} = 0$, which yields

$$S^{(1)} = \frac{1}{i\lambda}\sum_\alpha \frac{(-1)^\alpha}{i\lambda} P_\alpha V P_{\bar{\alpha}}. \tag{A5}$$

We note that, due to the structure of H_0, $[iS^{(1)}, H_0] + \sum_\alpha P_\alpha V P_{\bar{\alpha}} = 0$. Using $S^{(1)}$, we can find the effective Hamiltonian, for the two subspaces, up to second order:

$$\mathcal{H}_{\text{eff}} = e^{iS}(H_0 + V)e^{-iS} - H_0 \approx \sum_{\alpha=a,b} P_\alpha\Big(V + [iS^{(1)}, V] - \frac{1}{2}\{(S^{(1)})^2, H_0\} + S^{(1)}H_0S^{(1)}\Big)P_\alpha, \tag{A6}$$

where $\{f, g\}$ represents the anticommutator $fg + gf$.

If we are interested in the corrections to the wave functions, we need to know the unitary transformation e^{iS} up to second order. $S^{(2)}$ is found by solving $P_\alpha([iS^{(2)}, H_0] + [iS^{(1)}, V] - \frac{1}{2}\{(S^{(1)})^2, H_0\} + S^{(1)}H_0S^{(1)})P_{\tilde{\alpha}} = 0$, which yields

$$S^{(2)} = \frac{1}{i\lambda^2}\sum_\alpha P_\alpha V(P_\alpha - P_{\tilde{\alpha}})VP_{\tilde{\alpha}}. \tag{A7}$$

To make the RSRG-X method work, the Schrieffer-Wolff perturbation theory must converge. We infer from the above forms that a necessary condition is that the largest eigenvalue must be smaller in absolute value than λ: $||V|| \ll \lambda$. This should also be sufficient in most physical cases, but we do not attempt to pursue a proof of this notion, but rather rely on small-size numerics to confirm the validity of the method.

APPENDIX B: APPLICATION TO THE hJJ′ MODEL

The hJJ′ model naturally fits the mold of the RSRG-X model, just as the TFIM has become the ubiquitous example for the ground state RSRG method. Following the convention of Eq. (1), we write the site and bond terms, respectively, as

$$\mathcal{H}_i = -h_i\sigma_i^z, \qquad \mathcal{H}_{i+1/2} = -J_i\sigma_i^x\sigma_{i+1}^x - J_i'\sigma_i^z\sigma_{i+1}^z. \tag{B1}$$

We concentrate on the case in which J' is small and, therefore, can be treated perturbatively. In this case, the largest gap in the chain may arise either due to a site Hamiltonian, i.e., a large field h_i, or a bond Hamiltonian, i.e., a large Ising term J_i. For notational simplicity, we assume that the largest coupling occurs on site $i = 2$, and we refer to Figs. 2(c) and 2(d) for the definition of the notation. Applying the Schrieffer-Wolff transformation, we find the site dominant rule to be

$$\tilde{h}_1 \to h_1 + cJ_1', \qquad \tilde{h}_3 \to h_3 + cJ_2', \tag{B2}$$

$$\tilde{J}_1 \to c\frac{J_1J_2}{h_2}, \qquad \tilde{J}_1' \to 0, \tag{B3}$$

$$\lambda \to c\left(h_2 + \frac{J_1^2 + J_2^2}{2h_2}\right), \tag{B4}$$

and the bond dominant rule to be

$$\tilde{h}_1 \to h_1 + c\frac{h_2J_1'}{J_2}, \qquad \tilde{h}_c \to J_2' + c\frac{h_2h_3}{J_2},$$
$$\tilde{h}_4 \to h_4 + c\frac{h_3J_3'}{J_2}, \tag{B5}$$

$$\tilde{J}_1 \to cJ_1, \qquad \tilde{J}_c \to J_3, \tag{B6}$$

$$\tilde{J}_1' \to c\frac{h_3J_1'}{J_2}, \qquad \tilde{J}_c' \to c\frac{h_2J_3'}{J_2}, \tag{B7}$$

$$\lambda \to c\left(J_2 + \frac{h_2^2 + h_3^2 + (J_1')^2 + (J_3')^2}{2J_2}\right). \tag{B8}$$

Here, $c = \pm 1$ indicates the choice of the local Hilbert space (tree branch) and λ is the shift of the energy eigenvalue.

The most important thing in the RSRG-X procedure is that no relevant new terms are produced, and the decimation step could repeat itself until all degrees of freedom in the chain are accounted for.

APPENDIX C: NUMERICS

The RSRG-X procedure was performed numerically on random spin chains with length L from 500 to 2000 spins. For each realization of disorder, we performed $5 \times L$ equilibration Monte Carlo steps, followed by $2 \times (10^5$–$10^6))$ data collection Monte Carlo steps. The initial distributions for J_i, h_i, and J_i' were selected to be uniform distributions with the following ranges:

$$P[J] = U(0.3, 1 - s), \qquad P[h] = U(0.3, 1 + s),$$
$$P[J'] = U(0, \Delta_{J'}), \tag{C1}$$

where $U[a, b]$ indicates the uniform distribution that ranges from a to b, s is the initial shift of the distribution (which we translate into the initial value of the tuning parameter δ_I), and $\Delta_{J'}$ corresponds to the width of the initial J' distribution. We note that, while we only used positive-definite initial distributions of J and h, we looked at both positive-definite ($\Delta_{J'} > 0$) and negative-definite ($\Delta_{J'} < 0$) initial distributions of J'.

APPENDIX D: DERIVATION OF THE HEAT CONDUCTIVITY

To find the heat current operator, we apply the relation $j_i = [\sum_{k=1}^{i}\mathcal{H}_i, \mathcal{H}]$ to the TFIM model and obtain $j_i = -2iJ_ih_{i+1}\sigma_i^x\sigma_{i+1}^y$. Here, we do not include J' contributions because J' is an irrelevant operator that will not affect the low-frequency thermal conductivity. In order to compute the heat current operator at a given RG step, we use the renormalized Hamiltonian in the commutation relation. We note that using the Schrieffer-Wolff transformation on the heat current operator as we run the RG yields exactly the same result as the direct calculation using the renormalized Hamiltonian because the heat current operator is directly tied to the Hamiltonian.

To compute the thermal conductivity, we follow Ref. [28] and write the Kubo formula [Eq. (6)] in terms of an explicit trace over many-body eigenstates:

$$\kappa(\omega) = \frac{\pi}{\omega Z L}\sum_{m,n}\delta(\omega + E_m - E_n)e^{-\beta E_m} \times (1 - e^{-\beta\omega})|\langle n|\sum_i j_i|m\rangle|^2, \quad \text{(D1)}$$

where Z is the partition function. To evaluate κ using Monte Carlo methods, we sample over the states $|m\rangle$. To determine E_n and the matrix element $|\langle m|\sum_i j_i|n\rangle|$, we assume that the most important contribution comes from the local Hamiltonian that is being decimated at the scale ω. That is, if we are decimating the bond J_k, then $E_n = E_m - \omega \approx E_m - 2J_k$ and $|\langle m|\sum_i j_i|n\rangle| \approx 2J_k h_{k+1}$. Similarly, if we are decimating the site h_k, $E_n = E_m - 2h_k$ and $|\langle m|\sum_i j_i|n\rangle| \approx 2J_{k-1}h_k$.

In the noninteracting case, we can evaluate κ explicitly, as the partition function becomes a product of partition functions of the individual RG steps. Thus, we can explicitly write down the heat conductivity

$$\kappa(\omega) = \frac{1}{\omega}n(\omega)P(\omega;\omega)\int_0^{\omega} R(\omega';\omega)(2\omega\omega')^2 d\omega \tanh\left(\frac{\omega}{T}\right) + (P\leftrightarrow R), \quad \text{(D2)}$$

where $n(\omega)$ is the fraction of the sites that survive at the scale ω and $P(\cdot,\omega)$ $[R(\cdot,\omega)]$ is the distribution of $|J|$'s $[|h|$'s$]$ at scale ω. Using the critical and off-critical distributions from Ref. [[27]], we find

$$\kappa(\omega) \sim \begin{cases} \omega^{3+2|\delta|} & \omega < T \\ \omega^{2+2|\delta|} & \omega > T. \end{cases} \quad \text{(D3)}$$

We observe that the exponent at criticality can be obtained from the engineering dimensions using the following facts: the dimensionality of the heat current operator $[j_k(\omega)] \sim \omega^2$, the distribution functions $[P(\cdot;\omega)] = [R(\cdot;\omega)] = \omega^{-1}$, and remembering that $\tanh(\frac{\omega}{T})$ contributes a power of ω in the "hydrodynamic" regime $\omega \ll T$. The first logarithmic correction to this result is $\log(1/\omega)^{-4}$, where two powers of the logarithm come from the density of states, one power comes from the J distribution, and one power from the h distribution.

APPENDIX E: BENCHMARKING

Here, we benchmark our RSRG-X method against numerical and analytic solutions of free-fermion models and against exact diagonalization calculations on small hJJ' chains. Before starting, we note that the RSRG-X method is only asymptotically exact: as one performs RSRG-X steps and flows towards stronger disorder, the method becomes more accurate. Consequently, for the case of weak disorder, one can compare scaling properties, but direct comparisons of objects like many-body spectra are expected to work only for the case of strong disorder. First, we look at exactly solvable spin chains and make a comparison of scaling properties obtained from RSRG-X with those obtained from exact diagonalization and analytics. We then move on to the nonintegrable hJJ' spin chains and show that, in the limit of strong disorder, the RSRG-X becomes exact.

We begin by looking at the single-particle spectrum of long hJ spin chains. In particular, we are interested in the low-energy part of this spectrum as it is responsible for the low-frequency dynamical properties of the system such as the ac heat conductivity and the dynamic spin-correlation function. Generically, the effective couplings generated in each RSRG-X step depend on the branching choice. However, in the absence of interactions ($J' = 0$), the magnitude of the generated couplings becomes independent of the branching choice. Therefore, in the noninteracting case, we can associate each branching choice with a quasiparticle with the energy that corresponds to the splitting between the two choices. Eqs. (B4) and (B8). On the other hand, the exact single-particle excitation spectrum can also be obtained by converting the hJ model Hamiltonian into the free-fermion form

$$H = \sum_i J_i(c_i^\dagger c_{i+1}^\dagger + c_i^\dagger c_{i+1} + \text{H.c.}) + h_i(1 - 2c_i^\dagger c_{i+1}^\dagger) \quad \text{(E1)}$$

and finding the corresponding eigenvalues numerically.

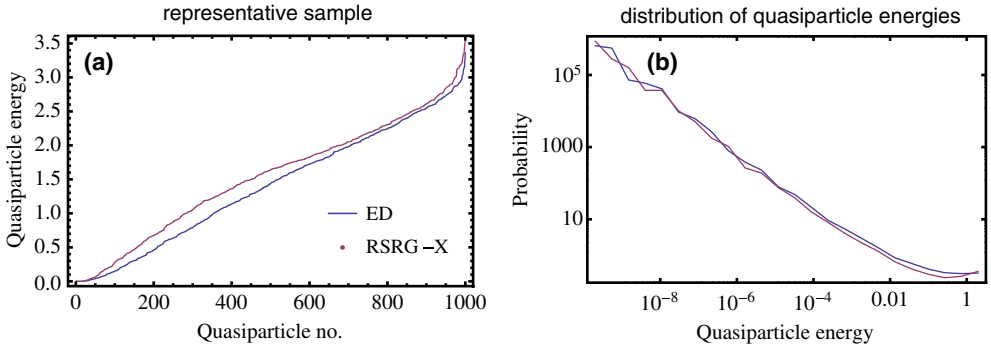

FIG. 5. (a) Comparison of the single quasiparticle spectrum for a representative 1000 spin hJ chain at criticality computed using RSRG-X and exact diagonalization (ED). (b) Comparison of the distribution of quasiparticle energies obtained using RSRG-X and ED for the hJ model. The data were obtained from 50 disorder realizations of 1000 spin chains at criticality.

To compare the single-particle RSRG-X spectrum with the exact one, we run the two methods on spin chains of 1000 spins. For the initial disorder distributions, we use flat distributions $P(J_i) = \theta(J_i)\theta(1 - J_i)$ and $P(h_i) = \theta(h_i)\theta(1 - h_i)$. Using identical distributions for the h_i's and J_i's ensures that the spin chain is critical and, thus, least local, which provides the most stringent test of the RSRG-X. In Fig. 5(a), we compare the average single-particle spectrum, for a collection of 50 disorder realizations, computed using the two different methods. We observe that there is some deviation between the two spectra at intermediate energies, but the low-energy excitations look quite similar.

To quantify the similarities between the single-particle spectra obtained using RSRG-X and exact diagonalization, we bin the eigenvalues obtained from the 50 disorder realizations and plot their probability distribution $P(\epsilon)$ [see Fig. 5(b)]. At low frequencies, we observe that the two methods obtain a nearly identical form of $P(\epsilon) \sim \epsilon^{\alpha-1}$ (with $\alpha \to 0$ at criticality). The mismatch between RSRG-X and ED is a consequence of the errors made by the RSRG-X in the initial part of the flow, before strong disorder is reached. The existence of the mismatch indicates that nonuniversal properties like T_c may not be accurately computed by RSRG-X. However, the fact that we obtain the correct low-frequency scaling form using the RSRG-X methods indicates that it should provide a good description of the universal low-frequency properties.

Next, we move to benchmarking RSRG-X applied to nonintegrable spin chains. In this case, the only reliable method at our disposal is ED. Since ED works only for very small systems, it cannot be used for investigating scaling properties. Instead, we focus on the more limited goal of showing that RSRG-X becomes asymptotically exact as we approach the strong disorder limit. To make the comparison, we focus on the many-body eigenspectra and the overlap of eigenfunctions. To set up the comparison, we must choose how to simulate strong disorder. We choose to use power-law initial distributions of the form $P(J) \sim J^{1/a-1}$, $P(h) \sim h^{1/b-1}$, where the constants a and b control the disorder strength (increasing a and b corresponds to stronger disorder). To ensures that either J or h but not J' is the largest

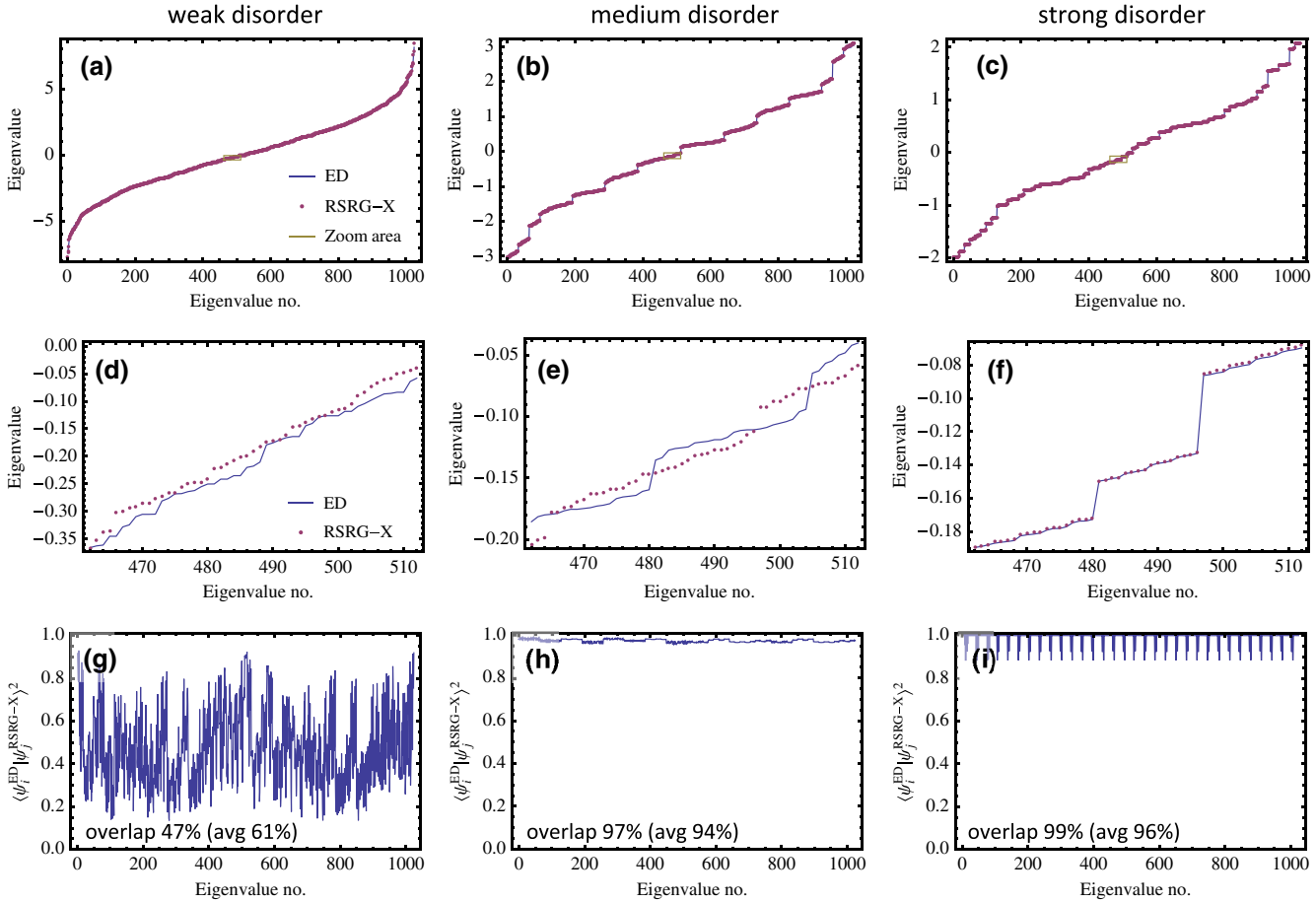

FIG. 6. (a)–(c) Comparison of the 1024 many-body eigenvalues computed using RSRG-X and ED for three representative 10-spin hJJ′ chains with weak, medium, and strong disorder. (d)–(f) Zoom in on spectra shown in (a)–(c). (g)–(i) Overlap of RSRG-X and ED eigenfunctions. The average overlap for the given disorder realization is indicated in the bottom of the figure (the disorder averaged overlap, frrm Fig. 7, is indicated in brackets). (See text for details.)

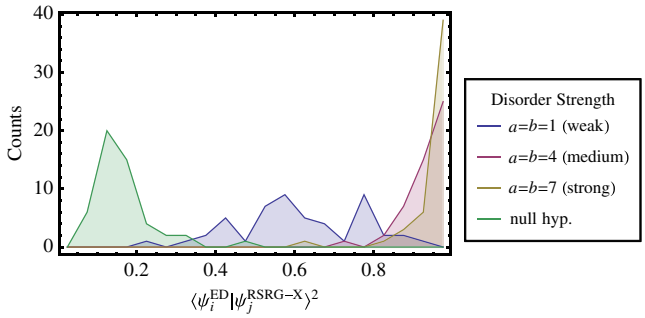

FIG. 7. Histogram of the average overlap of RSRG-X and ED eigenfunctions, computed for three values of disorder strength. Also shown is the histogram for the null hypothesis: average overlap of ED eigenfunctions computed for pairs of different disorder realizations. (See text for details.)

local coupling, we pick J_i' from a uniform distribution with the range $[(0\text{–}0.2)\max\{J_i, h_i, h_{i+1}\}]$. To systematically observe the influence of the disorder, we use three values of disorder strength: weak ($a = b = 1$), medium ($a = b = 4$), and strong ($a = b = 7$).

We compute the full many-body eigenspectra and the corresponding eigenfunctions for 10 site chains with weak, medium, and strong disorder using ED and RSRG-X. Comparing the many-body eigenspectra, Figs. 6(a)–6(c), we see that the spectra obtained by ED and RSRG-X look similar. Zooming in on the middle part of the spectrum, Figs. 6(d)–6(f), we observe that for weak disorder there is some difference in the ED and the RSRG-X spectrum; however, as the disorder strength increases, the ED and RSRG-X spectra match better and better. We also compare the overlap of the eigenfunctions computed using RSRG-X with those obtained using ED. In particular, for each RSRG-X eigenfunction ψ_i, we compute the overlap with the best matching ED eigenfunction ϕ_j (i.e., we maximize $\langle\psi_i|\phi_j\rangle^2$ over j's). We plot the resulting overlaps in Figs. 6(g)–6(i). We observe that even in the case of weak disorder, we find significant overlap, showing that RSRG-X is performing a good job of capturing the qualitative features of the eigenfunctions. As we crank up the disorder, we find that the overlap becomes extremely good for medium disorder and essentially perfect for strong disorder.

In order to quantify the quality of the eigenfunctions, we compute the overlap for 50 disorder realizations. For each disorder realization, we obtain the average overlap for each RSRG-X eigenfunction $\frac{1}{N}\sum_i \max_j[\langle\psi_i|\phi_j\rangle^2]$, and bin the results. In addition, as a null hypothesis, we take pairs of independent disorder realizations and compute the overlap between ED eigenstates of these pairs. The resulting histograms are plotted in Fig. 7. The histograms show that even for weak disorder we obtain significantly better overlap between ED and RSRG-X eigenfunctions, as compared to the null hypothesis. Moreover, the overlap becomes essentially perfect as the disorder strength is cranked up.

Here, we benchmark the RSRG-X method. In particular, we show by comparing the RSRG-X method with exact diagonalization that RSRG-X becomes essentially exact in the asymptotic limit of strong disorder. The strong disorder limit is precisely the regime that is needed for understanding the many-body localized state and its universal, low-frequency properties. Surprisingly, we also find that the RSRG-X can capture the essential features of the many-body eigenstates even at weak disorder, thus showing that it has some applicability even outside of the scaling regime that it was designed for.

[1] D. S. Fisher and D. A. Huse, *Ordered Phase of Short-Range Ising Spin Glasses*, Phys. Rev. Lett. **56**, 1601 (1986).
[2] D. S. Fisher and D. A. Huse, *Equilibrium Behavior of the Spin-Glass Ordered Phase*, Phys. Rev. B **38**, 386 (1988).
[3] L. van Hove, *Sur l'Integrale de Configuration pour les Systemes de Particules a Une Dimension*, Physica (Amsterdam) **16**, 137 (1950).
[4] L. D. Landau and E. M. Lifshitz, *Statistical Physics* (Pergamon Press, New York, 1959), translated from Russian by E. Peierls and R. F. Peierls.
[5] P. W. Anderson, *Absence of Diffusion in Certain Random Lattices*, Phys. Rev. **109**, 1492 (1958).
[6] D. M. Basko, I. L. Aleiner, and B. L. Altshuler, *Metal-Insulator Transition in a Weakly Interacting Many-Electron System with Localized Single-Particle States*, Ann. Phys. (Amsterdam) **321**, 1126 (2006).
[7] D. M. Basko, I. L. Aleiner, and B. L. Altshuler, *Possible Experimental Manifestations of the Many-Body Localization*, Phys. Rev. B **76**, 052203 (2007).
[8] N. Mott, *The Mobility Edge since 1967*, J. Phys. C **20**, 3075 (1987).
[9] I. L. Aleiner, B. L. Altshuler, and G. V. Shlyapnikov, *A Finite-Temperature Phase Transition for Disordered Weakly Interacting Bosons in One Dimension*, Nat. Phys. **6**, 900 (2010).
[10] V. Oganesyan and D. A. Huse, *Localization of Interacting Fermions at High Temperature*, Phys. Rev. B **75**, 155111 (2007).
[11] C. Monthus and T. Garel, *Many-Body Localization Transition in a Lattice Model of Interacting Fermions: Statistics of Renormalized Hoppings in Configuration Space*, Phys. Rev. B **81**, 134202 (2010).
[12] A. Pal and D. A. Huse, *Many-Body Localization Phase Transition*, Phys. Rev. B **82**, 174411 (2010).
[13] S. Iyer, V. Oganesyan, G. Refael, and D. A. Huse, *Many-Body Localization in a Quasiperiodic System*, Phys. Rev. B **87**, 134202 (2013).
[14] D. A. Huse, R. Nandkishore, V. Oganesyan, A. Pal, and S. L. Sondhi, *Localization Protected Quantum Order*, Phys. Rev. B **88**, 014206 (2013).
[15] S. Sachdev, *Quantum Phase Transitions* (Cambridge University Press, Cambridge, England, 2011), 2nd ed.
[16] A. Karahalios, A. Metavitsiadis, X. Zotos, A. Gorczyca, and P. Prelovsek, *Finite-Temperature Transport in Disordered Heisenberg Chains*, Phys. Rev. B **79**, 024425 (2009).

[17] O. S. Barisic and P. Prelovsek, *Conductivity in a Disordered One-Dimensional System of Interacting Fermions*, Phys. Rev. B **82**, 161106 (2010).

[18] T. C. Berkelbach, and D. R. Reichman, *Conductivity of Disordered Quantum Lattice Models at Infinite Temperature: Many-Body Localization*, Phys. Rev. B **81**, 224429 (2010).

[19] E. Khatami, M. Rigol, A. Relaño, and A. M. García-García, *Quantum Quenches in Disordered Systems: Approach to Thermal Equilibrium without a Typical Relaxation Time*, Phys. Rev. E **85**, 050102 (2012).

[20] H. Kim and D. A. Huse, *Ballistic Spreading of Entanglement in a Diffusive Nonintegrable System*, Phys. Rev. Lett. **111**, 127205 (2013).

[21] M. Serbyn, Z. Papić, and D. A. Abanin, *Local Conservation Laws and the Structure of the Many-Body Localized States*, Phys. Rev. Lett. **111**, 127201 (2013).

[22] M. Serbyn, Z. Papić, and D. A. Abanin, *Universal Slow Growth of Entanglement in Interacting Strongly Disordered Systems*, Phys. Rev. Lett. **110**, 260601 (2013).

[23] C. Dasgupta and S. K. Ma, *Low-Temperature Properties of the Random Heisenberg Antiferromagnetic Chain*, Phys. Rev. B **22**, 1305 (1980).

[24] R. N. Bhatt and P. A. Lee, *Scaling Studies of Highly Disordered Spin-*$1/2$ *Antiferromagnetic Systems*, Phys. Rev. Lett. **48**, 344 (1982).

[25] D. S. Fisher, *Random Transverse-Field Ising Spin Chains*, Phys. Rev. Lett. **69**, 534 (1992).

[26] D. S. Fisher, *Random Antiferromagnetic Quantum Spin Chains*, Phys. Rev. B **50**, 3799 (1994).

[27] D. S. Fisher, *Critical Behavior of Random Transverse-Field Ising Spin Chains*, Phys. Rev. B **51**, 6411 (1995).

[28] O. Motrunich, K. Damle, and D. A. Huse, *Dynamics and Transport in Random Quantum Systems Governed by Strong-Randomness Fixed Points*, Phys. Rev. B **63**, 134424 (2001).

[29] R. Vosk and E. Altman, *Many-Body Localization in One Dimension as a Dynamical Renormalization Group Fixed Point*, Phys. Rev. Lett. **110**, 067204 (2013).

[30] S. Popescu, A. J. Short, and A. Winter, *Entanglement and the Foundations of Statistical Mechanics*, Nat. Phys. **2**, 754 (2006).

[31] M. Rigol, V. Dunjko, and M. Olshanii, *Thermalization and Its Mechanism for Generic Isolated Quantum Systems*, Nature (London) **452**, 854 (2008).

[32] P. R. Zangara, A. D. Dente, A. Iucci, P. R. Levstein, and H. M. Pastawski, *Interaction-Disorder Competition in a Spin System Evaluated through the Loschmidt Echo*, Phys. Rev. B **88**, 195106 (2013).

[33] J. H. Bardarson, F. Pollmann, and J. E. Moore, *Unbounded Growth of Entanglement in Models of Many-Body Localization*, Phys. Rev. Lett. **109**, 017202 (2012).

[34] N. Metropolis, A. W. Rosenbluth, M. N. Rosenbluth, A. H. Teller, and E. Teller, *Equation of State Calculations by Fast Computing Machines*, J. Chem. Phys. **21**, 1087 (1953).

[35] In a finite system, the spins belonging to the largest cluster can collectively flip on an exponentially long time scale set by the system size. Therefore, one has to consider the analogous four-point correlator $[\![\langle\sigma_i^x(t)\sigma_i^x(0)\sigma_j^x(t)\sigma_j^x(0)\rangle_{\mathrm{Th}}]\!]$.

[36] Because of the squared expectation value, m_{EA} cannot be written in the form $\mathrm{tr}(\rho A)$, where ρ is the equilibrium density matrix and A is an operator.

[37] B. Swingle, *A Simple Model of Many-Body Localization*, arXiv:1307.0507.

[38] R. Vosk and E. Altman, *Dynamical Quantum Phase Transitions in Random Spin Chains*, arXiv:1307.3256.